

1 **Tertiary lymphoid structures induced by CXCL13-producing CD4<sup>+</sup> T cells increase tumor**  
2 **infiltrating CD8<sup>+</sup> T cells and B cells in ovarian cancer**

3

4 Masayo Ukita<sup>1</sup>, Junzo Hamanishi<sup>1</sup>, Hiroyuki Yoshitomi<sup>2,3</sup>, Koji Yamanoi<sup>1</sup>, Shiro Takamatsu<sup>1</sup>, Akihiko  
5 Ueda<sup>1</sup>, Haruka Suzuki<sup>1</sup>, Yuko Hosoe<sup>1</sup>, Yoko Furutake<sup>1</sup>, Mana Taki<sup>1</sup>, Kaoru Abiko<sup>4</sup>, Ken Yamaguchi<sup>1</sup>,  
6 Hidekatsu Nakai<sup>5</sup>, Tsukasa Baba<sup>6</sup>, Noriomi Matsumura<sup>5</sup>, Akihiko Yoshizawa<sup>7</sup>, Hideki Ueno<sup>2,3</sup>, Masaki  
7 Mandai<sup>1</sup>

8

9 <sup>1</sup>Department of Gynecology and Obstetrics, Kyoto University Graduate School of Medicine, Kyoto,  
10 Japan

11 <sup>2</sup>Department of immunology, Kyoto University Graduate School of Medicine, Kyoto, Japan

12 <sup>3</sup>Institute for the Advanced Study of Human Biology (ASHBi), Kyoto University, Kyoto, Japan

13 <sup>4</sup>Department of Obstetrics and Gynecology, National Hospital Organization Kyoto Medical Center,  
14 Kyoto, Japan

15 <sup>5</sup>Department of Obstetrics and Gynecology, Kindai University Faculty of Medicine, Osaka, Japan

16 <sup>6</sup>Department of Obstetrics and Gynecology, Iwate Medical University, Iwate, Japan

17 <sup>7</sup>Department of Diagnostic Pathology, Kyoto University Graduate School of Medicine, Kyoto, Japan

18

19 **Corresponding author**

20 Junzo Hamanishi, MD, PhD.

21 Department of Gynecology and Obstetrics, Kyoto University Graduate School of Medicine, 54  
22 Shogoin Kawaharacho, Sakyo-ku, Kyoto, Japan.

23 Tel.: +81-75-751-3269

24 E-mail: [jnkhmns@kuhp.kyoto-u.ac.jp](mailto:jnkhmns@kuhp.kyoto-u.ac.jp)

25

26 **Keywords** Tertiary lymphoid structures, CXCL13, Tumor microenvironment, Ovarian cancer

27

28 **Acknowledgement** We thank all the members of the Center for Anatomical, Pathological and Forensic  
29 Medical Research and Medical Research Support Center, Graduate School of Medicine, Kyoto  
30 University for preparing microscope slides.

31

32 **Contributors** MU designed and performed the experiments, analyzed the data, and wrote the  
33 manuscript. JH and HY designed and directed the study and edited the manuscript. ST performed  
34 statistical analyses and commented on the manuscript. HN and KA provided the clinical data. YH  
35 assisted with the experiments. AU, HS, YF, MT, KYaman, KA, KYamag, TB, NM, AY, HU, and MM  
36 provided advice on the experiments and commented on the manuscript.

37

38 **Funding** This work was supported by a Grant-in-Aid for Scientific Research (B) (Grant Number

39 JP18H02945), Grant-in-Aid for JSPS Research Fellow (Grant Number JP19J12595), Grant-in-Aid for  
40 Challenging Exploratory Research (Grant Number JP20K20610), Grant-in-Aid for Research Activity  
41 Start-up (Grant Number JP20K22810), and Grant-in-Aid for Scientific Research (C) (Grant Number  
42 JP21K09541).

43

44 **Ethics approval and consent to participate** This study was approved by Kyoto University Graduate  
45 School and Faculty of Medicine, Ethics Committee (G531), Ethics Committee of Kindai University  
46 Faculty of Medicine (27-182), and Ethics committee of the National Hospital Organization Kyoto  
47 Medical Center (19-081). Informed consent was obtained in the form of opt-out on the Web site for  
48 the patients at Kyoto University and Kindai University. Written informed consent was obtained from  
49 the patients at Kyoto Medical Center. Animal experiments were approved by the Kyoto University  
50 Animal Research Committee. This study was conducted according to Declaration of Helsinki  
51 principles.

52

53 **Competing interests** None declared.

54

55 **Date availability statement** The data analyzed in this study were previously deposited in the Gene  
56 Expression Omnibus (GEO) at GSE39204 and GSE55512 by our laboratory. All data relevant to the  
57 study are included in the article or uploaded as supplementary information.

58

59

60 **Abstract**

61 **Background:** Tertiary lymphoid structures (TLSs) are transient ectopic lymphoid aggregates whose  
62 formation might be caused by chronic inflammation states, such as cancer. The presence of TLS is  
63 associated with a favorable prognosis in most solid malignancies. The recognition of the relevance of  
64 TLS to cancer has led to a growing interest in TLS as an immunomodulatory target to enhance tumor  
65 immunity, although how TLSs are induced in the tumor microenvironment (TME) and how they affect  
66 patient survival are not well understood.

67 **Methods:** TLS distribution in relation to tumor infiltrating lymphocytes (TILs) and related gene  
68 expression were investigated in high grade serous ovarian cancer (HGSC) specimens. CXCL13  
69 expression, which is strongly associated with TLS, and its localization in immune cells, were examined.  
70 We explored the tumor microenvironment for CXCL13 secretion by adding various inflammatory  
71 cytokines *in vitro*. The induction of TLS by CXCL13 was examined in a mouse model of ovarian  
72 cancer.

73 **Results:** CXCL13 gene expression correlated with TLS formation and the infiltration of T cells and B  
74 cells, and was a favorable prognostic factor for HGSC patients. The coexistence of CD8<sup>+</sup> T cells and  
75 B-cell lineages in the TME was associated with a better prognosis of HGSC and was closely related to  
76 the presence of TLSs. CXCL13 expression was predominantly coincident with CD4<sup>+</sup> T cells in TLSs  
77 and CD8<sup>+</sup> T cells in TILs, and shifted from CD4<sup>+</sup> T cells to CD21<sup>+</sup> follicular dendritic cells as the TLS  
78 matured. Although TGF- $\beta$  was reported to stimulate CXCL13 production, our *in vitro* results revealed

79 that CXCL13 secretion was promoted in CD4<sup>+</sup> T cells under TGF- $\beta$  + IL-2-restricted conditions and  
80 in CD8<sup>+</sup> T cells under TGF- $\beta$  + IL-12-rich conditions. In a mouse model of ovarian cancer,  
81 recombinant CXCL13 induced TLSs and enhanced survival by the infiltration of CD8<sup>+</sup> T cells.

82 **Conclusions:** TLS formation was promoted by CXCL13-producing CD4<sup>+</sup> T cells and TLSs facilitated  
83 the coordinated antitumor responses of cellular and humoral immunity in ovarian cancer.

84

## 85 **Background**

86 It is generally considered that the generation and regulation of an efficient adaptive immune response  
87 to cancer occurs in secondary lymphoid organs (SLOs) such as the regional lymph nodes. Antitumor  
88 immune cells are educated to recognize tumor antigens, proliferate in regional lymph nodes away from  
89 the tumor site, and then migrate into the tumor microenvironment (TME) to exert antitumor activity  
90 (1). Clinical studies have shown that higher densities of T cell subsets within the TME are associated  
91 with improved patient survival in several cancers including ovarian cancer (2-5). We previously  
92 reported that the forced infiltration of CD8<sup>+</sup> T cells into the TME by CCL19, a chemokine that attracts  
93 T cells, suppressed tumors in an ovarian cancer model (6). These results indicate that T cells have a  
94 critical role in the TME and that the TME might be a therapeutic target if effectively altered by  
95 immune-activating signals such as chemokines. To date, strategies to enhance the clinical efficacy of  
96 anti-tumor treatments have predominantly focused on the T cell component in the tumor, and the roles  
97 of other immune cell components have not been fully elucidated.

98 Recent studies have revealed an alternative immune response at the tumor site within SLO-like  
99 cellular aggregates called tertiary lymphoid structures (TLSs) (7). TLSs are transient ectopic lymphoid  
100 aggregates whose formation might be caused by chronic inflammation states, including autoimmune  
101 and infectious diseases, transplanted organ rejection, and cancer (7-9). The presence of TLS is  
102 associated with a favorable prognosis in most solid malignancies (10). Recently, it was reported that  
103 TLS-associated B cells synergized with T cells to contribute anti-tumor effects and that the presence  
104 of TLS and B cells in tumor sites enhanced the efficacy of immunotherapy (11-14). The recognition of  
105 the relevance of TLS to cancer has led to a growing interest in TLS as an immunomodulatory target to  
106 enhance tumor immunity, although how this can be induced therapeutically is not known.

107 The chemokines CXCL13, CCL19, and CCL21 are involved in lymphoid tissue-inducer (LTi) cell  
108 homing and lymph node development (8). Especially, CXCL13 was reported to be essential for the  
109 initial attraction of LTi cells and the formation of early lymph nodes (15). Although TLSs are thought  
110 to share the mechanisms of initial development with SLOs, TLS formation is distinct from the  
111 preprogrammed processes involved in SLOs and does not necessarily occur in all patients. The  
112 generation of TLS in inflamed tissues might be governed by specific inflammatory signals that have  
113 not been fully identified (7). In autoimmune diseases such as rheumatoid arthritis (RA), we showed  
114 that TGF- $\beta$  and other proinflammatory cytokines enhanced CXCL13 production by CD4<sup>+</sup> T cells, and  
115 that CXCL13-producing CD4<sup>+</sup> T cells had an important role in the formation of TLS (16, 17). However,

116 whether the same mechanism can be applied to the case of malignant tumors including ovarian cancer  
117 has not been investigated.

118 In this study, we assessed the relationship between tumor infiltrating T or B cells subsets and the  
119 presence of TLS, and evaluated the prognostic impact of TLS in ovarian cancer. We also investigated  
120 whether CXCL13 promoted TLS formation and improved the prognosis of patients with ovarian cancer.  
121 The role of CXCL13-producing CD4<sup>+</sup> T cells in the generation of TLS was also investigated.

122

## 123 **Methods**

### 124 **Human samples**

125 Sixty-two and 35 high grade serous ovarian cancer (HGSC) patients who underwent primary surgery  
126 at Kyoto University Hospital from 1997 to 2015 and at Kindai University Hospital from 2009 to 2016,  
127 respectively, were enrolled. Their clinical characteristics are described in Supplemental Table S1.  
128 Patients who received chemotherapy or radiation therapy prior to surgery were excluded. Four other  
129 patients with typical TLSs who underwent initial surgery at the National Hospital Organization Kyoto  
130 Medical Center between 2017 and 2019 were also included in the study.

131

### 132 **Immunohistochemical analysis and evaluation**

133 Immunohistochemical (IHC) staining was performed using formalin-fixed, paraffin-embedded  
134 (FFPE) specimens obtained from the above patients by the streptavidin-biotin-peroxidase method as

135 previously described (4, 6). The samples were incubated with anti-CD8, anti-CD4, anti-CD20, anti-  
136 CD38, and anti-CD21 antibodies. The antibodies used are listed in Supplemental Table S2.

137 Two independent investigators trained in the pathology of ovarian cancer and blinded to the clinical  
138 data examined the H&E staining and IHC slides. TLSs were evaluated by H&E staining and CD20  
139 positive cell aggregation as an indicator. Five sections at 400× magnification with the most abundant  
140 infiltration were manually counted and the mean count was calculated for CD8<sup>+</sup> T cells, CD4<sup>+</sup> T cells,  
141 and CD20<sup>+</sup> B cells. These immune cells in TLSs were not counted as tumor infiltrating lymphocytes  
142 (TILs). If their count was above the median, we defined them as CD8-high, CD4-high, and CD20-high  
143 tumor, respectively. Tumor infiltrated CD38<sup>+</sup> plasma cells were graded according to their intensity and  
144 fraction of positive cells as 0, 1, 2, or 3 (plasma cell score) according to previous reports (18,19). Cases  
145 with scores of 0 and 1 were defined as plasma cell-low tumor, and cases with scores of 2 and 3 were  
146 defined as plasma cell-high tumors.

147

#### 148 **Detection of CXCL13 mRNA by RNA ISH**

149 We assessed CXCL13 by RNA in situ hybridization (ISH) (RNAscope<sup>®</sup> 2.5 HD Reagent kit (RED),  
150 Advanced Cell Diagnostics, Hayward, CA, USA). FFPE tissue sections were deparaffinized in xylene  
151 and subsequently dehydrated in an ethanol series. Tissue sections were incubated in target retrieval  
152 reagent at 100°C for 15 minutes, and then treated with protease at 40°C for 30 minutes. Hybridization  
153 with Hs-CXCL13 (for human) or Mm-Cxcl13 (for mouse) probes at 40°C for 2 hours, and the amplifier

154 and visualization (Fast RED) procedures were performed in accordance with the manufacturer's  
155 instructions. For multiplex detection using FFPE, an RNAscope® Fluorescent Multiplex Reagent kit  
156 v2 (Advanced Cell Diagnostics) was used. Double staining was performed for CXCL13 and CD8,  
157 CXCL13 and CD4, and CXCL13 and CD21(CR2). The target probes and reagents used were listed in  
158 Supplemental Table S2. CXCL13 was detected with Opal 690, and CD4, CD8, and CR2 with Opal  
159 570. Fluorescence images were captured using a fluorescence microscope BZ-X800E (KEYENCE,  
160 Osaka, Japan), and the colocalization of CXCL13 with various immune cells was quantified using BZ-  
161 H4C/hybrid cell count software (KEYENCE).

162

### 163 **HGSC gene expression analysis**

164 HGSC specimens obtained from 28 patients who underwent primary surgery at Kyoto University  
165 Hospital from 1997 to 2012 were prepared for gene expression microarray analysis (KOV). The data  
166 were previously deposited in the Gene Expression Omnibus (Accession Numbers: GSE 39204 and  
167 GSE 55512).

168 The gene expression profile of the TCGA-OV RNA sequencing dataset (n=217) from The Cancer

169 Genome Atlas (TCGA) Data Portal (<http://cancergenome.nih.gov>,

170 illuminahisec\_maseqv2\_Level\_3\_RSEM\_genes\_normalized\_data files obtained and merged on 19,

171 Oct, 2015) was used for survival analysis and correlation testing among CXCL13, TGF-β1, PDCD1,

172 and CD274.



173

174 **Gene expression and infiltrating immune cells analysis**

175 Raw gene expression microarray data using Affymetrix HT\_HG-U133A from TCGA ovarian serous  
176 cystadenocarcinoma samples were obtained from the GDC legacy archive  
177 (<https://portal.gdc.cancer.gov/legacy-archive/>) in the form of CEL files (n=522). Gene expression  
178 values were calculated by normalization using the RMA method with R package “affy” ([http://www.R-](http://www.R-project.org)  
179 [project.org](http://www.R-project.org)). Subsequently, the relative abundance of 22 immune cell types for each sample was  
180 estimated using CIBERSORT (<http://cibersort.stanford.edu/>).

181

182 **T cell receptor (TCR) and B cell receptor (BCR) repertoire analysis**

183 TLSs and tumor areas were identified by microscopy and macrodissected independently from FFPE  
184 sections (Supplemental Figure S1C). RNA was extracted using NucleoSpin® total RNA FFPE (Takara  
185 Bio, Shiga, Japan) according to the manufacturer’s instructions. Sequencing of the TCR $\alpha$  (TRA) and  
186 BCR IgG heavy chain loci were performed at Repertoire Genesis Incorporation (Osaka, Japan) using  
187 an unbiased amplification method with MiSeq (Illumina, San Diego, CA, USA). Data processing,  
188 assignment, and aggregation were performed using a repertoire analysis software program, Repertoire  
189 Genesis (RG), provided by Repertoire Genesis Incorporation. RG assigns TRV and TRJ alleles to  
190 queries and then generates CDR3 sequences, finally aggregating their combination patterns.

191

192 **Induction assay of CXCL13 in CD4<sup>+</sup> and CD8<sup>+</sup> T cells**

193 PBMCs from healthy donors were collected using Lymphocyte Separation Solution 1.077 (Nacalai  
194 Tesque, Kyoto, Japan). Blood CD8<sup>+</sup> T cells were isolated with CD8 MicroBeads, human (Miltenyi  
195 Biotec, Bergisch Gladbach, NRW, Germany). Blood CD4<sup>+</sup> T cells were purified with a Naïve CD4<sup>+</sup> T  
196 cell isolation kit II, human (Miltenyi Biotec) through a magnetic column.

197 Human T cells were differentiated for 6–7 days in a humidified 5% CO<sub>2</sub> incubator at 37°C with  
198 IMDM (Thermo Fisher, Waltham, MA, USA) supplemented with 10% fetal bovine serum, 100  
199 units/ml penicillin and streptomycin under stimulation with 5 µg/ml plate-bound CD3 monoclonal  
200 antibody (clone: OKT3, Thermo Fisher) and 10 µg/ml CD28 monoclonal antibody (clone: CD28.2,  
201 Thermo Fisher) in the presence of 10 ng/ml TGF-β1 (Cell Signaling Technology, Danvers, MA, USA)  
202 unless otherwise described. Human T cells were also cultured under conditions where 5 µg/ml  
203 neutralizing anti-IL-2 antibody (R&D Systems, Minneapolis, MN, USA) or 10 ng/ml IL-12  
204 (PeproTech, Montreal, Quebec, Canada) was added.

205 Human T cells were cultured under CD3/CD28 stimulation using conditioned medium from the  
206 human serous ovarian cancer cell lines: OVCA420, OVCA433, and DK-09. OVCA420 and OVCA433  
207 were kindly provided by Dr. Susan K. Murphy of Duke University. DK-09 is a cell line that we  
208 established from the ascites of a patient with recurrent ovarian cancer (see Supplemental Methods). To  
209 block the TGF-β signals, a TGF-β signal inhibitor, SB431542 (Stemgent, Beltsville, MD, USA) was  
210 added at 0.5 and 5 µM.

211

## 212 **Flow cytometry**

213 For intracellular staining, cells were cultured for 4 hours with 4  $\mu$ M monensin (Sigma-Aldrich, Saint  
214 Louis, MO, USA), fixed, and stained with eBioscience™ Intracellular Fixation & Permeabilization  
215 Buffer Set (Thermo Fisher) and antibodies for intracellular molecules. Fixable Viability Dye eFluor  
216 506 (Thermo Fisher) was used to exclude dead cells. To detect CXCL13, CXCR5 and PD-1, the  
217 antibodies listed in supplemental table S2 were used. Data were acquired using MACS Quant Analyzer  
218 10 (Miltenyi Biotec) and were analyzed with FlowJo 10.0 (FlowJo LLC, Ashland, OR, USA).

219

## 220 **ELISA**

221 The concentrations of CXCL13 and TGF- $\beta$ 1 in the supernatant were measured with the respective  
222 kits listed in Supplemental Table S2.

223

## 224 **Cell lines and tumor models**

225 The OV2944-HM-1(HM-1) mouse ovarian cancer cell line was purchased from RIKEN BioResource  
226 Center (Ibaraki, Japan) and cultured as described (20). Throughout the study, we used HM-1 cell lines  
227 passaged fewer than 20 times, and regularly tested for mycoplasma contamination. Female B6C3F1  
228 (C57BL6  $\times$  C3/He F1) mice and nude mice (BALB/C-nu: CAnN.Cg-*Foxn1*<sup>tmu</sup>/Crl) were purchased  
229 from Charles River Japan (Yokohama, Japan), and were maintained under specific pathogen-free

230 conditions.

231 A total of  $1 \times 10^6$  HM-1 cells were inoculated intraperitoneally into B6C3F1 mice. Mouse  
232 recombinant CXCL13 (R&D Systems) treatment was initiated one day after the tumor inoculation and  
233 administered intraperitoneally at 1  $\mu\text{g}/\text{mouse}$  every other day for five times. Control mice received  
234 PBS intraperitoneally. Then, 10–12 days after inoculating the tumor, mice were euthanized with carbon  
235 dioxide and the formation of TLS in omental tumors was analyzed.

236 A total of  $2.5 \times 10^5$  HM-1 cells were inoculated intraperitoneally into B6C3F1 and nude mice.  
237 Similarly, rCXCL13 (1  $\mu\text{g}/\text{mouse}$ ) and anti-PD-L1 antibody (200  $\mu\text{g}/\text{mouse}$ ) were intraperitoneally  
238 administered 5 times every other day starting from day 1 and day 3, respectively, after tumor  
239 implantation. Anti-PD-L1 antibody (clone 10F.9G2, Bio X Cell, Lebanon, NH, USA) and Rat IgG  
240 antibody (clone LFT-2, Bio X Cell) were used as negative controls.

241

#### 242 **IHC analysis of mouse tumors**

243 Mouse tumor cryosections (6- $\mu\text{m}$ -thick) were stained with anti-CD4, anti-CD8 (clone YTS169.4),  
244 anti-CD19, and anti-Ki-67 antibodies as previously described (21). The antibodies are listed in  
245 Supplemental Table S2. Mouse FFPE specimens were stained with anti-CD8 antibody (clone  
246 EPR20305).

247

#### 248 **Statistics**

249 Results are shown as the mean  $\pm$  SEM from at least three independent experiments unless otherwise  
250 stated. A *P* value of less than 0.05 was considered statistically significant. Significance was calculated  
251 using the 2-tailed Student's *t*-test, and correlation between groups was determined by Spearman's  
252 correlation test. The log-rank test was used for overall survival analysis unless otherwise described.  
253 All statistical analyses were performed using GraphPad Prism 7 (GraphPad software, San Diego, CA,  
254 USA). The Jonckheere-Terpstra test was performed using the "clinfun" packages in R.

255

## 256 **Results**

### 257 **TLS is associated with intratumor infiltration by CD8<sup>+</sup> T cells and B-cell lineages and is closely** 258 **related to a favorable prognosis**

259 The prognostic significance of the respective infiltration of T cell and B cell subsets was investigated  
260 by the IHC analysis of initial surgical specimens of HGSC (n=97) (Supplemental Table S1). Patients  
261 with a higher infiltration of CD8<sup>+</sup> T cells, CD20<sup>+</sup> B cells, and CD38<sup>+</sup> plasma cells had significantly  
262 prolonged progression free survival than those with low numbers of infiltrating cells (*P*<0.05, each)  
263 (Figure 1A). In addition, there was a significant correlation between the infiltrated number of CD8<sup>+</sup> T  
264 cells and B-cell lineage cells (Figure 1B), and patients with a higher number of infiltrated CD8<sup>+</sup> T cells  
265 and B-cell lineages had the best prognosis (Figure 1C). The intratumoral infiltration of CD8<sup>+</sup> T cells  
266 or B-cell lineages alone did not contribute to the improved prognosis.

267 H&E and IHC staining evaluation of TLSs in the same samples (n=97) revealed that 61 patients

268 (62.9%) had TLSs (Supplemental Table S1, Supplemental Figure S1, A and B). In the cases with TLS,  
269 the number of infiltrating CD8<sup>+</sup> T cells, CD4<sup>+</sup> T cells, CD20<sup>+</sup> B cells, or CD38<sup>+</sup> plasma cells (plasma  
270 cell score) was significantly higher than in those without TLS ( $P<0.0001$ , each) (Figure 1D). Focusing  
271 on the pattern of tumor infiltrating lymphocytes and the presence of TLS, TLS were found in 94% of  
272 cases with a high infiltration of CD8<sup>+</sup> T cells and B-cell lineages (CD8 high-CD20 high: n=35, CD8  
273 high-plasma cell high: n=32) (Figure 1E). The close relationship between TLS and the distribution of  
274 infiltrating CD8<sup>+</sup> T cell and B-cell lineages suggests that cellular and humoral immunity interact via  
275 the TLS in ovarian cancer.

276 Next, we performed TCR and BCR repertoire analysis using tumor sections from HGSC patients  
277 (n=3), separating TLS and TIL regions by macrodissection (Supplemental Figure S1C). In two of three  
278 cases, TCR repertoire analysis showed many clones distributed in the TIL, whereas oligoclonal  
279 amplification was observed in TLS. Furthermore, the clone with the highest amplification from TIL  
280 was consistent with the clone observed in TLS (Figure 1F), suggesting that antigen-specific T cells  
281 that proliferated in TLS might also infiltrate into the tumor as TIL.

282 Patients with TLS, which is closely associated with intratumoral infiltration of CD8<sup>+</sup> T cells and B-  
283 cell lineages and may mediate cellular and humoral immunity, had a significantly better prognosis than  
284 patients without TLS (Wilcoxon test  $P=0.0016$ , median overall survival [110 months vs 70 months])  
285 (Figure 1G).

286

287 **CXCL13 gene expression in tumors correlates with TLS formation, lymphocyte infiltration, and**  
288 **a favorable prognosis for ovarian cancer**

289 The expression of CXCL13 analyzed by RNA ISH demonstrated CXCL13 was highly expressed in  
290 TLS (Figure 2A). In addition, there were cases in which immune cells in the tumor stroma also  
291 expressed high levels of CXCL13 (Supplemental Figure S2A). From the IHC of initial surgical  
292 specimens with our original microarray data (KOV: GSE39204/55512, n=28), the ratio of cases with  
293 TLS was significantly higher in those with high CXCL13 gene expression than in those with low  
294 CXCL13 gene expression in tumor specimens ( $P=0.046$ ) (Figure 2B). Additionally, CXCL13 gene  
295 expression was significantly correlated with the numbers of several types of TILs such as CD4<sup>+</sup> and  
296 CD8<sup>+</sup> T cells, CD20<sup>+</sup> B cells and CD38<sup>+</sup> plasma cells ( $P<0.001$ , each) (Figure 2C, Supplemental Figure  
297 S2B).

298 To validate these data, we applied CIBERSORT to examine the distribution of infiltrating immune  
299 cells into tumor sites and CXCL13 gene expression using the RNA sequence data of ovarian cancer  
300 cases registered in TCGA. The infiltration of CD8<sup>+</sup> T cells had the strongest correlation with CXCL13  
301 gene expression, and that of CD4<sup>+</sup> T cells, CD20<sup>+</sup> B cells, CD38<sup>+</sup> plasma cells and M1-macrophages  
302 also showed a strong correlation with CXCL13 gene expression, while that of M2-macrophages and  
303 mature dendritic cells were negatively correlated, and that of natural killer cells and regulatory T  
304 (Treg) cells were not correlated with CXCL13 gene expression (Figure 2, D and E, Supplemental  
305 Figure S2, C and D). These results suggest that CXCL13 gene expression strongly correlated with the

306 formation of TLS and the number of tumor-infiltrating T cells and B-cell lineages.

307 Next, we examined the impact of CXCL13 on the prognosis of HGSC and found that patients with  
308 high CXCL13 gene expression had a significantly better prognosis in the KOV data and TCGA data  
309 ( $P < 0.05$ , each) (Figure 2F).

310  
311 **CXCL13 produced by CD4<sup>+</sup> T cells is critical for TLS initiation**

312 To identify cells producing CXCL13 involved in TLS formation, we performed RNA ISH double  
313 staining (CXCL13 and CD4<sup>+</sup> T cells, CXCL13 and CD8<sup>+</sup> T cells) using HGSC tumor specimens. In  
314 the TLS region, CXCL13 was highly coexpressed with CD4<sup>+</sup> T cells, whereas CD8<sup>+</sup> T cells  
315 predominantly expressed CXCL13 in the tumor and stromal regions (Figure 3, A and B).

316 HGSC tissues contain two types of TLSs: early TLS, in which lymphocytes aggregate diffusely and  
317 CD21<sup>+</sup> cells are scarce, and follicle-formed TLS, which has the follicular morphology of SLO and  
318 where CD21<sup>+</sup> follicular dendritic cells (FDCs) are distributed in a reticular pattern (Figure 4, A and B).  
319 Therefore, we performed the double staining of CXCL13 and CD8<sup>+</sup> T cells, CXCL13 and CD4<sup>+</sup> T cells,  
320 and CXCL13 and CD21<sup>+</sup> FDCs by RNA ISH for representative early TLS and follicle-formed TLS.  
321 CXCL13 expression was highly consistent with CD4<sup>+</sup> cells in early TLSs, whereas few CD4<sup>+</sup> T cells  
322 expressing CXCL13 were observed in follicle-formed TLSs and CXCL13 expression was highly  
323 consistent with spindle-shaped CD21<sup>+</sup> FDCs (Figure 4C). These results indicate that CXCL13-  
324 producing CD4<sup>+</sup> T cells are closely related to the early stage of TLS formation.



325

### 326 **TGF- $\beta$ promotes the production of CXCL13**

327 To investigate which factors promote CXCL13 secretion from CD4<sup>+</sup> T cells and CD8<sup>+</sup> T cells, we  
328 analyzed two sets of gene expression data from ovarian cancer tissues. Using the TCGA RNA sequence  
329 data and our KOV microarray data, we found a significant correlation between CXCL13 and TGF- $\beta$ 1  
330 gene expression ( $P < 0.05$ ) (Figure 5A). The analysis of naïve CD4<sup>+</sup> T cells and CD8<sup>+</sup> T cells isolated  
331 from the peripheral blood cells of a healthy donor and cultured with TGF- $\beta$  showed that CD4<sup>+</sup> T cells  
332 predominantly secreted CXCL13 compared with CD8<sup>+</sup> T cells. A TGF- $\beta$  signal inhibitor (SB431542)  
333 suppressed the secretion of CXCL13 in a concentration-dependent manner (Figure 5B).

334 We previously reported that the TGF- $\beta$  signaling pathway was activated in ovarian cancer (22), and  
335 we detected high concentrations of TGF- $\beta$ 1 in the conditioned medium of three different human  
336 ovarian cancer cell lines (Figure 5C). Using these conditioned media, we examined their effects on  
337 CXCL13 production in naïve CD4<sup>+</sup> and CD8<sup>+</sup> T cells. In CD4<sup>+</sup> T cells, CXCL13 secretion was  
338 promoted in the order of TGF- $\beta$ 1 concentration, and was suppressed in a concentration-dependent  
339 manner when incubated with the TGF- $\beta$  signal inhibitor (SB431542) (Figure 5D). However, TGF- $\beta$ -  
340 mediated CXCL13 secretion in CD8<sup>+</sup> T cells was limited.

341 Next, we conducted similar experiments by adding various cytokines to TGF- $\beta$  to reproduce the TME.  
342 We found that CXCL13 secretion was enhanced in CD4<sup>+</sup> T cells under IL-2-restricted conditions and  
343 in CD8<sup>+</sup> T cells under IL-12-enriched conditions (Figure 5E). The CXCL13 concentration in the

344 culture supernatant showed a similar trend (Figure 5F). CXCL13-producing CD4<sup>+</sup> cells had a PD-1  
345 positive, CXCR5 negative phenotype (Figure 5G). These results suggest that the phase and TME in  
346 which CD4<sup>+</sup> and CD8<sup>+</sup> T cells produce CXCL13 are different, and thus CD4<sup>+</sup> T cells may produce  
347 CXCL13 in TLSs and CD8<sup>+</sup> T cells in TILs (Figure 3, A and B).

348

### 349 **Mouse recombinant CXCL13 induces TLS in tumors and prolongs survival**

350 The effect of CXCL13 on TLS formation in tumors was analyzed using a mouse ovarian cancer model.  
351 A mouse ovarian cancer cell line HM-1 was intraperitoneally inoculated to B6C3F1 immunocompetent  
352 mice, and mouse recombinant(r) CXCL13 was intraperitoneally administered 5 times every other day  
353 starting from day 1, and TLS formed in the omental tumor were evaluated on days 10–12. The area of  
354 TLSs per tumor area was significantly increased in the rCXCL13-treated group compared with the  
355 control group (Figure 6A). IHC revealed that mouse TLS, similar to human TLS, consisted mainly of  
356 CD19<sup>+</sup> B cells, and that CD8<sup>+</sup> T cells and CD4<sup>+</sup> T cells were present in and around TLSs. Furthermore,  
357 TLSs contained many Ki-67 positive immune cells indicating these structures were immunologically  
358 activated (Supplemental Figure S3A). Furthermore, CXCL13 was highly expressed and corresponding  
359 with TLSs (Figure 6B). The administration of rCXCL13 markedly increased the infiltration of CD8<sup>+</sup>  
360 T cells around the TLSs (Figure 6C).

361 Next, we observed the effect of rCXCL13 administration on the survival of mice. In  
362 immunocompetent mice (B6C3F1), the survival time was significantly prolonged in the rCXCL13-

363 treated group compared with the control group (Figure 6D). Because there was a correlation between  
364 CXCL13 and PD-1/PD-L1 gene expression (Supplemental Figure S3B), we hypothesized that  
365 CXCL13 had an adjuvant effect in HM-1 ovarian cancer models that were originally refractory to anti-  
366 PD-1/PD-L1 antibody therapy. However, no significant prognostic improvement was observed  
367 (Supplemental Figure S3C).

368 Furthermore, the administration of rCXCL13 to immunocompromised mice (nude mice) did not  
369 improve survival (Figure 6E). Consistent with the apparent increase in CD8<sup>+</sup> T cells around the TLSs  
370 in immunocompetent mice, CXCL13 contributed to their improved survival via immunity. These  
371 results indicate that CXCL13 induced TLSs and TILs, indicating CXCL13 and TLS might be new  
372 therapeutic targets for ovarian cancer.

373

## 374 **Discussion**

375 We showed that the presence of TLS was associated with an increased intratumor infiltration of CD8<sup>+</sup>  
376 T cells and B-cell lineages, and that CD8<sup>+</sup> T cells and B-cell lineages might cooperate to improve the  
377 prognosis of ovarian cancer. It was reported that tumor infiltrating B cells contributed to tumor growth  
378 and progression through the production of cytokines, such as IL-10, that inhibit antitumor immunity  
379 although the functional role of B cells in cancer is poorly understood (23). Recently, there have been  
380 increasing numbers of reports that the presence of B cells, especially those associated with TLSs, may  
381 improve cancer outcomes (10, 12-14). Tumors containing CD8<sup>+</sup> T cells and B-cell lineages were

382 associated with improved prognosis in melanoma, sarcoma, and ovarian cancer (12, 13, 18). In this  
383 study, we found a strong correlation between the infiltrated numbers of CD8<sup>+</sup> T cells and B-cell  
384 lineages, and confirmed the presence of TLS in 94% of patients with tumors containing high numbers  
385 of infiltrated T and B cells. These results suggest that B-cell lineages are an essential component of the  
386 CD8<sup>+</sup> T cell cytotoxic reaction, and that cellular and humoral immune interactions are mediated by  
387 TLSs.

388 Whether tumor-associated TLSs are formed in response to a series of chronic inflammation or  
389 whether they are induced as a tumor antigen-specific immune response has not been fully established.  
390 De Chaisemartin et al. demonstrated that TLSs provided the specialized vasculature and  
391 chemoattractants necessary for T cell infiltration into non-small cell lung cancer (NSCLC) (24). The  
392 TCR repertoire analysis of NSCLC showed that the expansion of T cell clones in the tumor bed and  
393 peripheral blood correlated with the density of tumor associated TLSs (25). In this study, TCR  
394 repertoire analysis of the TLSs and tumor regions revealed that oligoclonal expansion occurred in TLS  
395 and that the same clone was highly amplified in the tumor. These data suggest that the recognition of  
396 antigens occurs in TLS and that the effector T cell clones amplified by the TLS infiltrate into tumors,  
397 both of which might provide evidence that TLS promotes immune responses in TME.

398 High CXCL13 gene expression was associated with disease activity and pathogenicity in autoimmune  
399 diseases such as RA (26-28), and with patients' prognosis in several types of cancer (7, 29, 30),  
400 implying the strong involvement of CXCL13-dependent TLS formation. In line with previous reports,

401 CXCL13 gene expression is a prognostic factor for ovarian cancer and is strongly associated with the  
402 formation of TLS. The presence of TLS also improved the long-term prognosis of ovarian cancer.

403 We previously reported that CXCL13-producing PD-1 high CXCR5 negative CD4<sup>+</sup> T cells have an  
404 important role in the function of TLS in RA (16, 17). Although FDCs are the main source of CXCL13  
405 in SLOs (31), the origin of CXCL13 in tumor associated TLS depends on the type of cancer. CXCL13  
406 was secreted by PD-1<sup>high</sup> CD8<sup>+</sup> T cells in lung cancer (32), by CD103<sup>+</sup> CD8<sup>+</sup> cells in ovarian cancer  
407 (33), and by CXCR5<sup>-</sup> PD-1<sup>high</sup> CD4<sup>+</sup> follicular helper like T cells in breast cancer (34). In this study,  
408 CXCL13 was predominantly expressed on CD4<sup>+</sup> T cells in TLSs and on CD8<sup>+</sup> and CD4<sup>+</sup> T cells in  
409 TILs, and that the expression of CXCL13 in TLSs shifted from CD4<sup>+</sup> T cells to CD21<sup>+</sup> FDCs.

410 Sequential stages of the development in tumor-associated TLS were observed in lung cancer. Siliņa et  
411 al. defined three types of TLSs: early TLS (E-TLS) without FDCs or germinal centers (GC), primary  
412 follicle like TLS (PFL-TLS) with an FDC network and lacking GC, and secondary follicle like TLS  
413 (SFL-TLS) with an FDC network and GC formation (35). Our data suggest that CXCL13-producing  
414 CD4<sup>+</sup> T cells are an important primary producer of CXCL13 in the early stages of TLS when FDCs  
415 are not present. FDCs emerge from ubiquitous perivascular mesenchymal cells expressing platelet-  
416 derived growth factor receptor  $\beta$  (36). CXCL13 itself directly induces lymphotoxin (LT) production  
417 by naïve B cells, and this CXCL13/LT pathway is crucial for FDC differentiation (37-39). We consider  
418 that FDC becomes the main source of CXCL13 in TLSs after the FDC network is formed, similar to  
419 that in SLOs.

420 The CXCL13-producing PD-1 high CXCR5 negative CD4<sup>+</sup> T cells we reported in RA (16, 17) do not  
421 express CXCR5, a marker typical of follicular helper T cells (Tfh). In the current study, the CD4<sup>+</sup> T  
422 cells in which CXCL13 expression was induced were PD-1 high CXCR5 negative. The CXCL13-  
423 producing CD4<sup>+</sup> T cells reported in breast cancer (34) had similar characteristics. The comprehensive  
424 analysis of blood and synovial samples of RA patients was used to propose a pathogenic PD-1<sup>high</sup>  
425 CXCR5<sup>-</sup> CD4 subset as peripheral helper T cells (Tph) (40, 41). Tph cells express factors that enable  
426 B-cell help, including IL-21, CXCL13, and ICOS. Similar to PD-1<sup>high</sup>-CXCR5<sup>+</sup> Tfh, Tph cells induce  
427 plasma cell differentiation *in vitro* through IL-21 secretion and SLAMF5 interactions (40). In this  
428 context, CXCL13-producing CD4<sup>+</sup> T cells not only promote the initial formation of TLSs but may also  
429 support anti-tumor antibody responses by B cells. Evidence for this was shown in our study, where B-  
430 cell lineages were clearly increased in patients with TLS and were associated with an improved  
431 prognosis. However, further research related to the co-localization of antigen-specific B cells with Tph  
432 cells in TLSs is warranted at the molecular level.

433 Proinflammatory conditions involving TGF- $\beta$  promoted the differentiation of CXCL13-producing  
434 CD4<sup>+</sup> T cells in our previous studies (16, 17) and in breast and ovarian cancers (33, 34). Resident  
435 fibroblasts and macrophages, and infiltrating Tregs produce TGF- $\beta$  locally (42). Previously, we  
436 reported that the TGF- $\beta$  signaling pathway was activated in advanced ovarian cancer and promoted  
437 tumor progression and metastasis (22). Indeed, high levels of TGF- $\beta$ 1 were detected in the conditioned  
438 medium of DK-09, a cell line we established from the ascites of a recurrent multidrug-resistant HGSC

439 patient. In this study, we performed a CXCL13 induction assay using PBMCs from a healthy donor  
440 and found that TGF- $\beta$  promoted CXCL13 secretion, although there was a significant difference in  
441 response to TGF- $\beta$  between CD4<sup>+</sup> T cells and CD8<sup>+</sup> T cells. Furthermore, CXCL13 production was  
442 enhanced in CD4<sup>+</sup> T cells under an IL-2 restricted environment and in CD8<sup>+</sup> T cells under an IL-12  
443 rich environment.

444 In addition to TGF- $\beta$ , IL-2 is involved in the differentiation of CD4<sup>+</sup> T cells. Quenching IL-2 by Treg  
445 or dendritic cells was reported to contribute to the differentiation of Tfh and Th17 cells (43, 44). In our  
446 previous studies, an IL-2 neutralizing antibody enhanced CXCL13 production by PD-1<sup>high</sup> CXCR5<sup>-</sup>  
447 CD4<sup>+</sup> T cells in RA (16, 17). Gu-Trantien et al. reported that IL-2 deprivation was critical for the  
448 production of CXCL13 and the accumulation of activated Tregs in parallel with CXCL13<sup>+</sup>CD4<sup>+</sup> TIL  
449 in breast cancer (34). However, IL-12 produced by dendritic cells and macrophages has an essential  
450 role in the interactions between the innate and adaptive immune systems. IL-12 promotes CD8<sup>+</sup>  
451 cytotoxic T cell activation and expansion (45-47). Our findings that the secretory environment of  
452 CXCL13 was different between CD4<sup>+</sup> and CD8<sup>+</sup> T cells is interesting and consistent with the different  
453 predominance of cells expressing CXCL13 between TLSs and TILs in ovarian cancer tumor sections.  
454 The environment of CXCL13 production differs between CD4<sup>+</sup> and CD8<sup>+</sup> T cells, and their roles in  
455 the formation and maintenance of TLSs may be different, and should be studied in future experiments.  
456 Last, we evaluated whether TLS was induced by CXCL13. In a mouse model of spontaneously  
457 developing gastric cancer by activated STAT3 signaling, chemokines, CXCL13, CCL19, and CCL21

458 were induced simultaneously with tumorigenesis and TLS formation (48). We administered mouse  
459 rCXCL13 one day after tumor inoculation and succeeded in inducing TLSs. CXCL13 was highly  
460 expressed and corresponding with TLSs. CXCL13 signals B cells to enhance LT production (37, 49),  
461 and the exogenous CXCL13 may have promoted a positive feed-forward loop. In the CXCL13 treated  
462 group, the infiltration of CD8<sup>+</sup> T cells around the TLS was clearly increased, and the survival time of  
463 tumor-bearing mice was also prolonged. Direct antitumor effects by CXCL13 were also observed in a  
464 colon cancer model. However, tumor growth was accelerated in CXCR5 or Rag1 knockout mice (30).  
465 The CXCL13 axis is a functional part of the relevant immune control and the TME can be altered by  
466 inducing CXCL13 and TLSs. Accordingly, our results clearly demonstrate that the induction of  
467 CXCL13 and TLSs has potential as an immune-modulatory target for ovarian cancer.

468 Taken together, CXCL13 is a strong prognostic factor for ovarian cancer, and is highly involved in  
469 the formation of TLS. CXCL13-producing CD4<sup>+</sup> T cells induced by TGF- $\beta$  under an IL-2 restricted  
470 tumor environment are important for the initial formation of TLS. The presence of TLS mobilizes  
471 various lymphocytes, and in particular, the simultaneous infiltration of B-cell lineages that are critical  
472 for the cytotoxic response of CD8<sup>+</sup> T cells in ovarian cancer. The strong interaction between humoral  
473 and cellular immunity in the antitumor response was revealed, and the possibility of TLS-mediated  
474 interactions was demonstrated. *In vivo* experiments revealed the TME can be altered by inducing  
475 CXCL13 and TLSs, which might be an important immunomodulatory method to enhance antitumor  
476 immunity.



477

478 **References**

- 479 1. Mellman I, Coukos G, and Dranoff G. Cancer immunotherapy comes of age. *Nature*.  
480 2011;480(7378):480-9.
- 481 2. Zhang L, Conejo-Garcia JR, Katsaros D, Gimotty PA, Massobrio M, Regnani G, et al.  
482 Intratumoral T Cells, Recurrence, and Survival in Epithelial Ovarian Cancer. *N Engl J Med*.  
483 2003;348(3):203-13.
- 484 3. Fridman WH, Zitvogel L, Sautès-Fridman C, and Kroemer G. The immune contexture in  
485 cancer prognosis and treatment. *Nat Rev Clin Oncol*. 2017;14(12):717-34.
- 486 4. Hamanishi J, Mandai M, Iwasaki M, Okazaki T, Tanaka Y, Yamaguchi K, et al. Programmed  
487 cell death 1 ligand 1 and tumor-infiltrating CD8+ T lymphocytes are prognostic factors of  
488 human ovarian cancer. *Proc Natl Acad Sci U S A*. 2007;104(9):3360-5.
- 489 5. Abiko K, Mandai M, Hamanishi J, Yoshioka Y, Matsumura N, Baba T, et al. PD-L1 on Tumor  
490 Cells Is Induced in Ascites and Promotes Peritoneal Dissemination of Ovarian Cancer through  
491 CTL Dysfunction. *Clin Cancer Res*. 2013;19(6):1363-74.
- 492 6. Hamanishi J, Mandai M, Matsumura N, Baba T, Yamaguchi K, Fujii S, et al. Activated Local  
493 Immunity by CCL19-Transduced Embryonic Endothelial Progenitor Cells Suppresses  
494 Metastasis of Murine Ovarian Cancer. *Stem Cells*. 2010;28(1):164–173.
- 495 7. Pitzalis C, Jones GW, Bombardieri M, and Jones SA. Ectopic lymphoid-like structures in

- 496 infection, cancer and autoimmunity. *Nat Rev Immunol*. 2014;14(7):447-62.
- 497 8. Aloisi F, and Pujol-Borrell R. Lymphoid neogenesis in chronic inflammatory diseases. *Nat Rev*  
498 *Immunol*. 2006;6(3):205-17.
- 499 9. Jing F, and Choi EY. Potential of Cells and Cytokines/Chemokines to Regulate Tertiary  
500 Lymphoid Structures in Human Diseases. *Immune Netw*. 2016;16(5):271-80.
- 501 10. Sautes-Fridman C, Petitprez F, Calderaro J, and Fridman WH. Tertiary lymphoid structures in  
502 the era of cancer immunotherapy. *Nat Rev Cancer*. 2019;19(6):307-25.
- 503 11. Bruno TC. New predictors for immunotherapy responses sharpen our view of the tumour  
504 microenvironment. *Nature*. 2020;577(7791):474-6.
- 505 12. Cabrita R, Lauss M, Sanna A, Donia M, Skaarup Larsen M, Mitra S, et al. Tertiary lymphoid  
506 structures improve immunotherapy and survival in melanoma. *Nature*. 2020;577(7791):561-5.
- 507 13. Petitprez F, de Reynies A, Keung EZ, Chen TW, Sun CM, Calderaro J, et al. B cells are  
508 associated with survival and immunotherapy response in sarcoma. *Nature*.  
509 2020;577(7791):556-60.
- 510 14. Helmink BA, Reddy SM, Gao J, Zhang S, Basar R, Thakur R, et al. B cells and tertiary  
511 lymphoid structures promote immunotherapy response. *Nature*. 2020.
- 512 15. Van De Pavert SA, Olivier BJ, Goverse G, Vondenhoff MF, Greuter M, Beke P, et al.  
513 Chemokine CXCL13 is essential for lymph node initiation and is induced by retinoic acid and  
514 neuronal stimulation. *Nat Immunol*. 2009;10(11):1193-9.

- 515 16. Kobayashi S, Watanabe T, Suzuki R, Furu M, Ito H, Ito J, et al. TGF-beta induces the  
516 differentiation of human CXCL13-producing CD4(+) T cells. *Eur J Immunol.* 2016;46(2):360-  
517 71.
- 518 17. Yoshitomi H, Kobayashi S, Miyagawa-Hayashino A, Okahata A, Doi K, Nishitani K, et al.  
519 Human Sox4 facilitates the development of CXCL13-producing helper T cells in inflammatory  
520 environments. *Nat Commun.* 2018;9(1):3762.
- 521 18. Kroeger DR, Milne K, and Nelson BH. Tumor-Infiltrating Plasma Cells Are Associated with  
522 Tertiary Lymphoid Structures, Cytolytic T-Cell Responses, and Superior Prognosis in Ovarian  
523 Cancer. *Clin Cancer Res.* 2016;22(12):3005-15.
- 524 19. Lohr M, Edlund K, Botling J, Hammad S, Hellwig B, Othman A, et al. The prognostic  
525 relevance of tumour-infiltrating plasma cells and immunoglobulin kappa C indicates an  
526 important role of the humoral immune response in non-small cell lung cancer. *Cancer Lett.*  
527 2013;333(2):222-8.
- 528 20. Peng J, Hamanishi J, Matsumura N, Abiko K, Murat K, Baba T, et al. Chemotherapy Induces  
529 Programmed Cell Death-Ligand 1 Overexpression via the Nuclear Factor- $\kappa$ B to Foster an  
530 Immunosuppressive Tumor Microenvironment in Ovarian Cancer. *Cancer Res.*  
531 2015;75(23):5034-45.
- 532 21. Horikawa N, Abiko K, Matsumura N, Hamanishi J, Baba T, Yamaguchi K, et al. Expression  
533 of Vascular Endothelial Growth Factor in Ovarian Cancer Inhibits Tumor Immunity through

- 534 the Accumulation of Myeloid-Derived Suppressor Cells. *Clin Cancer Res.* 2017;23(2):587-99.
- 535 22. Yamamura S, Matsumura N, Mandai M, Huang Z, Oura T, Baba T, et al. The activated  
536 transforming growth factor-beta signaling pathway in peritoneal metastases is a potential  
537 therapeutic target in ovarian cancer. *Int J Cancer.* 2012;130(1):20-8.
- 538 23. Yuen GJ, Demissie E, and Pillai S. B Lymphocytes and Cancer: A Love–Hate Relationship.  
539 *Trends Cancer.* 2016;2(12):747-57.
- 540 24. De Chaisemartin L, Goc J, Damotte D, Validire P, Magdeleinat P, Alifano M, et al.  
541 Characterization of Chemokines and Adhesion Molecules Associated with T cell Presence in  
542 Tertiary Lymphoid Structures in Human Lung Cancer. *Cancer Res.* 2011;71(20):6391-9.
- 543 25. Zhu W, Germain C, Liu Z, Sebastian Y, Devi P, Knockaert S, et al. A high density of tertiary  
544 lymphoid structure B cells in lung tumors is associated with increased CD4+T cell receptor  
545 repertoire clonality. *OncoImmunology.* 2015;4(12):e1051922.
- 546 26. Takemura S, Braun A, Crowson C, Kurtin PJ, Cofield RH, O’Fallon WM, et al. Lymphoid  
547 Neogenesis in Rheumatoid Synovitis. *J Immunol.* 2001;167(2):1072-80.
- 548 27. Shi K, Hayashida K, Kaneko M, Hashimoto J, Tomita T, Lipsky PE, et al. Lymphoid  
549 Chemokine B Cell-Attracting Chemokine-1 (CXCL13) Is Expressed in Germinal Center of  
550 Ectopic Lymphoid Follicles Within the Synovium of Chronic Arthritis Patients. *J Immunol.*  
551 2001;166(1):650-5.
- 552 28. Wutte N, Kovacs G, Berghold A, Reiter H, Aberer W, and Aberer E. CXCL13 and B-cell

- 553           activating factor as putative biomarkers in systemic sclerosis. *Br J Dermatol.* 2013;169(3):723-
- 554           5.
- 555   29.   Gu-Trantien C, Loi S, Garaud S, Equeter C, Libin M, de Wind A, et al. CD4(+) follicular helper
- 556           T cell infiltration predicts breast cancer survival. *J Clin Invest.* 2013;123(7):2873-92.
- 557   30.   Bindea G, Mlecnik B, Tosolini M, Kirilovsky A, Waldner M, Anna, et al. Spatiotemporal
- 558           Dynamics of Intratumoral Immune Cells Reveal the Immune Landscape in Human Cancer.
- 559           *Immunity.* 2013;39(4):782-95.
- 560   31.   Gunn MD, Ngo VN, Ansel KM, Ekland EH, Cyster JG, and Williams LT. A B-cell-homing
- 561           chemokine made in lymphoid follicles activates Burkitt's lymphoma receptor-1. *Nature.*
- 562           1998;391(6669):799-803.
- 563   32.   Thommen DS, Koelzer VH, Herzig P, Roller A, Trefny M, Dimeloe S, et al. A transcriptionally
- 564           and functionally distinct PD-1+ CD8+ T cell pool with predictive potential in non-small-cell
- 565           lung cancer treated with PD-1 blockade. *Nat Med.* 2018;24(7):994-1004.
- 566   33.   Workel HH, Lubbers JM, Arnold R, Prins TM, Van Der Vlies P, De Lange K, et al. A
- 567           Transcriptionally Distinct CXCL13+CD103+CD8+ T-cell Population Is Associated with B-
- 568           cell Recruitment and Neoantigen Load in Human Cancer. *Cancer Immunol Res.* 2019;7(5):784-
- 569           96.
- 570   34.   Gu-Trantien C, Migliori E, Buisseret L, De Wind A, Brohée S, Garaud S, et al. CXCL13-
- 571           producing TFH cells link immune suppression and adaptive memory in human breast cancer.

572 *JCI Insight*. 2017;2(11).

573 35. Siliņa K, Soltermann A, Attar FM, Casanova R, Uckeley ZM, Thut H, et al. Germinal Centers  
574 Determine the Prognostic Relevance of Tertiary Lymphoid Structures and Are Impaired by  
575 Corticosteroids in Lung Squamous Cell Carcinoma. *Cancer Res*. 2018;78(5):1308-20.

576 36. Krautler NJ, Kana V, Kranich J, Tian Y, Perera D, Lemm D, et al. Follicular Dendritic Cells  
577 Emerge from Ubiquitous Perivascular Precursors. *Cell*. 2012;150(1):194-206.

578 37. Aguzzi A, Kranich J, and Krautler NJ. Follicular dendritic cells: origin, phenotype, and  
579 function in health and disease. *Trends Immunol*. 2014;35(3):105-13.

580 38. Allen CDC, and Cyster JG. Follicular dendritic cell networks of primary follicles and germinal  
581 centers: Phenotype and function. *Semin Immunol*. 2008;20(1):14-25.

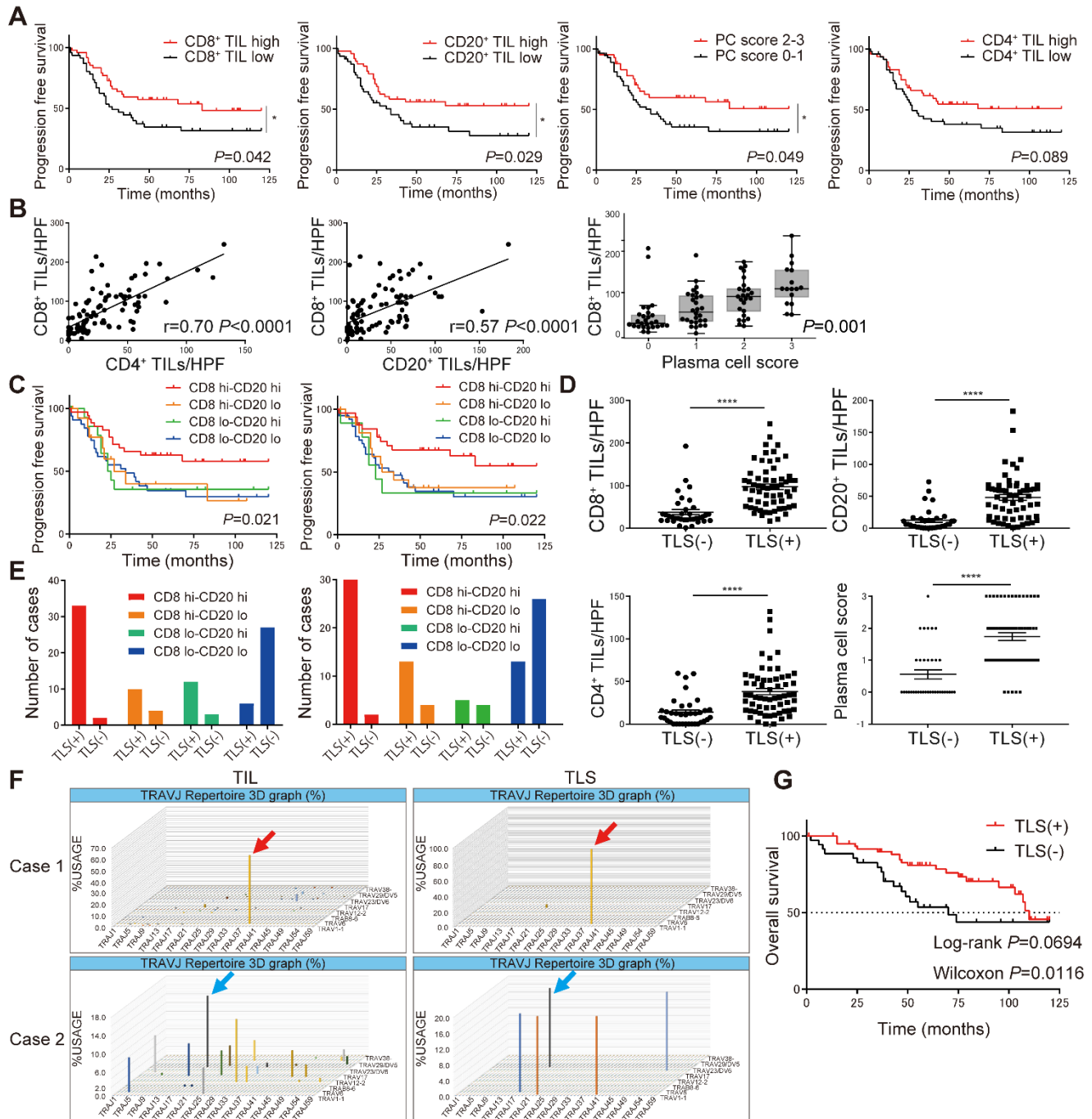
582 39. Fleige H, Ravens S, Moschovakis GL, Bölter J, Willenzon S, Sutter G, et al. IL-17–induced  
583 CXCL12 recruits B cells and induces follicle formation in BALT in the absence of  
584 differentiated FDCs. *J Exp Med*. 2014;211(4):643-51.

585 40. Rao DA, Gurish MF, Marshall JL, Slowikowski K, Fonseka CY, Liu Y, et al. Pathologically  
586 expanded peripheral T helper cell subset drives B cells in rheumatoid arthritis. *Nature*.  
587 2017;542(7639):110-4.

588 41. Yoshitomi H. CXCL13-producing PD-1hiCXCR5– helper T cells in chronic inflammation.  
589 *Immunol Med*. 2020;43(4):156-60.

590 42. Huang M, Sharma S, Zhu LX, Keane MP, Luo J, Zhang L, et al. IL-7 inhibits fibroblast TGF-

- 591  $\beta$  production and signaling in pulmonary fibrosis. *J Clin Invest.* 2002;109(7):931–937.
- 592 43. Liu Z, Gerner MY, Van Panhuys N, Levine AG, Rudensky AY, and Germain RN. Immune  
593 homeostasis enforced by co-localized effector and regulatory T cells. *Nature.*  
594 2015;528(7581):225-30.
- 595 44. Li J, Lu E, Yi T, and Cyster JG. EB12 augments Tfh cell fate by promoting interaction with IL-  
596 2-quenching dendritic cells. *Nature.* 2016;533(7601):110-4.
- 597 45. Teng MW, Bowman EP, McElwee JJ, Smyth MJ, Casanova JL, Cooper AM, et al. IL-12 and  
598 IL-23 cytokines: from discovery to targeted therapies for immune-mediated inflammatory  
599 diseases. *Nat Med.* 2015;21(7):719-29.
- 600 46. Colombo MP, and Trinchieri G. Interleukin-12 in anti-tumor immunity and immunotherapy.  
601 *Cytokine Growth Factor Rev.* 2002;13(2):155-68.
- 602 47. Lin L, Rayman P, Pavicic PG, Tannenbaum C, Hamilton T, Montero A, et al. Ex vivo  
603 conditioning with IL-12 protects tumor-infiltrating CD8<sup>+</sup> T cells from negative regulation by  
604 local IFN- $\gamma$ . *Cancer Immunol Immunother.* 2019;68(3):395-405.
- 605 48. Hill DG, Yu L, Gao H, Balic JJ, West A, Oshima H, et al. Hyperactive gp130/STAT3-driven  
606 gastric tumorigenesis promotes submucosal tertiary lymphoid structure development. *Int J*  
607 *Cancer.* 2018;143(1):167-78.
- 608 49. Aguzzi A, and Krautler NJ. Characterizing follicular dendritic cells: A progress report. *Eur J*  
609 *Immunol.* 2010;40(8):2134-8.

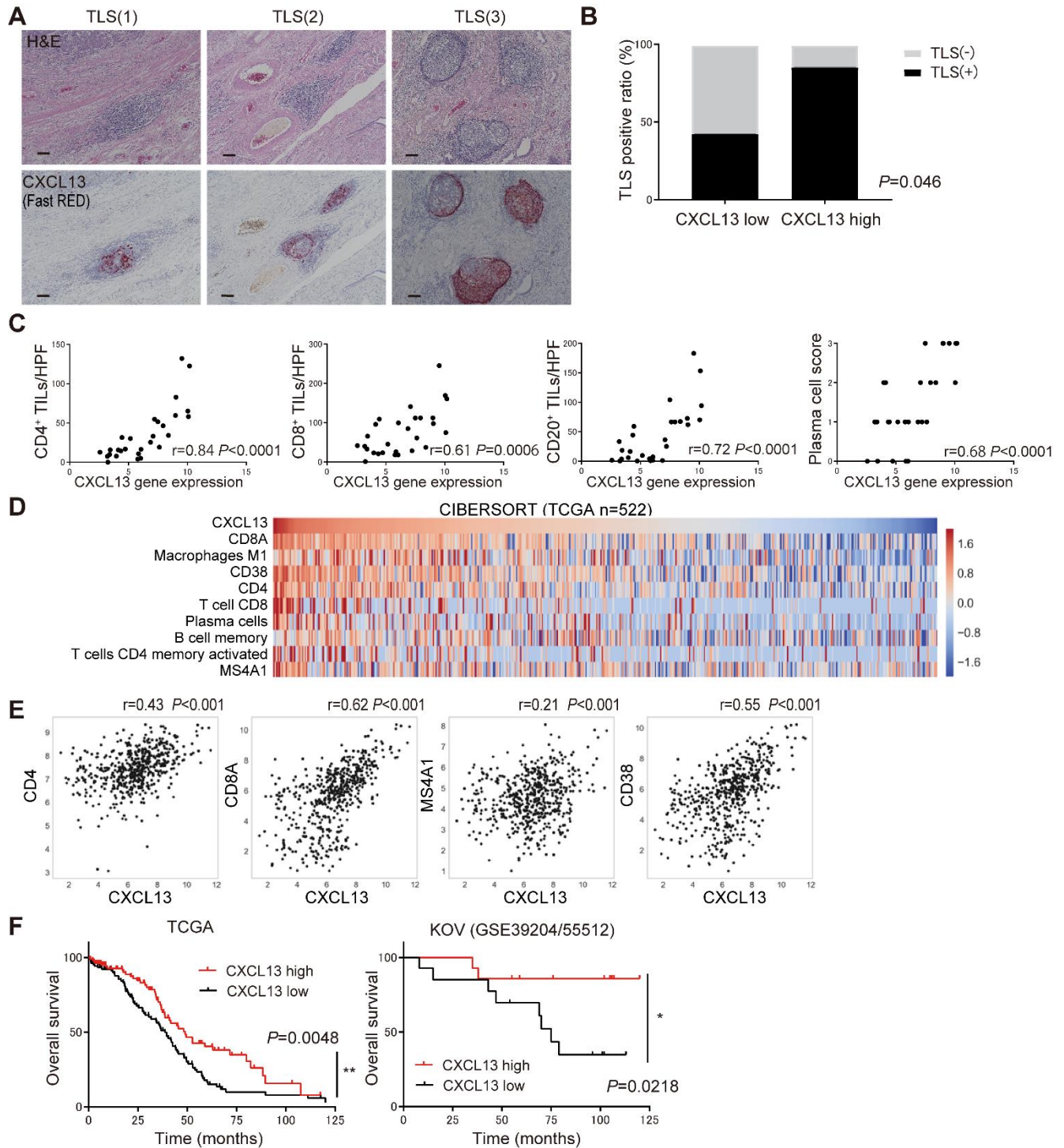


610

611 **Figure 1. TLS is associated with intratumor infiltration by CD8<sup>+</sup> T cells and B-cell lineages and is closely**  
 612 **related to a favorable prognosis. (A)** Progression free survival of the cohort stratified by CD8<sup>+</sup> T cells, CD20<sup>+</sup> B  
 613 cells, plasma cells (PC), and CD4<sup>+</sup> T cells (n=97, each). **(B)** Association between infiltrated numbers of CD4<sup>+</sup> T cells  
 614 and CD8<sup>+</sup> T cells, and CD8<sup>+</sup> T cells and B cell lineages in tumors (n=97). Correlations were determined by Pearson's  
 615 correlation test and Jonckheere-Terpstra trend tests. **(C)** Progression free survival of patients based on the tumor-  
 616 infiltrating CD8<sup>+</sup> T cells and B lineage cells (CD8 hi-CD20 hi: n=35, CD8 hi-CD20 lo: n=14, CD8 lo-CD20 hi: n=15,  
 617 CD8 lo-CD20 lo: n=33, total n=97) (CD8 hi-PC hi: n=32, CD8 hi-PC lo: n=17, CD8 lo-PC hi: n=9, CD8 lo-PC lo:  
 618 n=39, total n=97). **(D)** The number of tumor-infiltrating CD8<sup>+</sup> T cells, CD20<sup>+</sup> B cells, plasma cells, and CD4<sup>+</sup> T cells  
 619 according to TLS presence (TLS<sup>-</sup> n=36, TLS<sup>+</sup> n=61). *P* values were determined by Mann-Whitney *U*-test. **(E)**



620 Distribution of TLS in relation to the infiltration pattern of immune cells in tumors. Tumors were considered high  
621 (hi) for CD8<sup>+</sup> T cells, CD20<sup>+</sup> B cells and CD4<sup>+</sup> T cells if their score was above the median. Tumors were divided into  
622 two groups for PC by plasma cell score (0–1 n=56, 2–3 n=41), with 0–1 defined as PC low (lo) and 2–3 as PC hi in  
623 (A), (C), and (E). **(F)** TCR repertoire analysis separating TLS and TIL regions. The horizontal axis shows the J gene,  
624 the depth shows the V gene, and the vertical axis shows the frequency of usage. Clones indicated by arrows of the  
625 same color confirm the same amino acid sequence of CDR3. **(G)** Overall survival of patients with HGSC by the  
626 presence of TLS (TLS<sup>-</sup> n=36, TLS<sup>+</sup> n=61, total n=97). Analyses were performed with Kaplan-Meier estimates and  
627 log-rank tests in (A) (C), and Wilcoxon tests (G).  
628

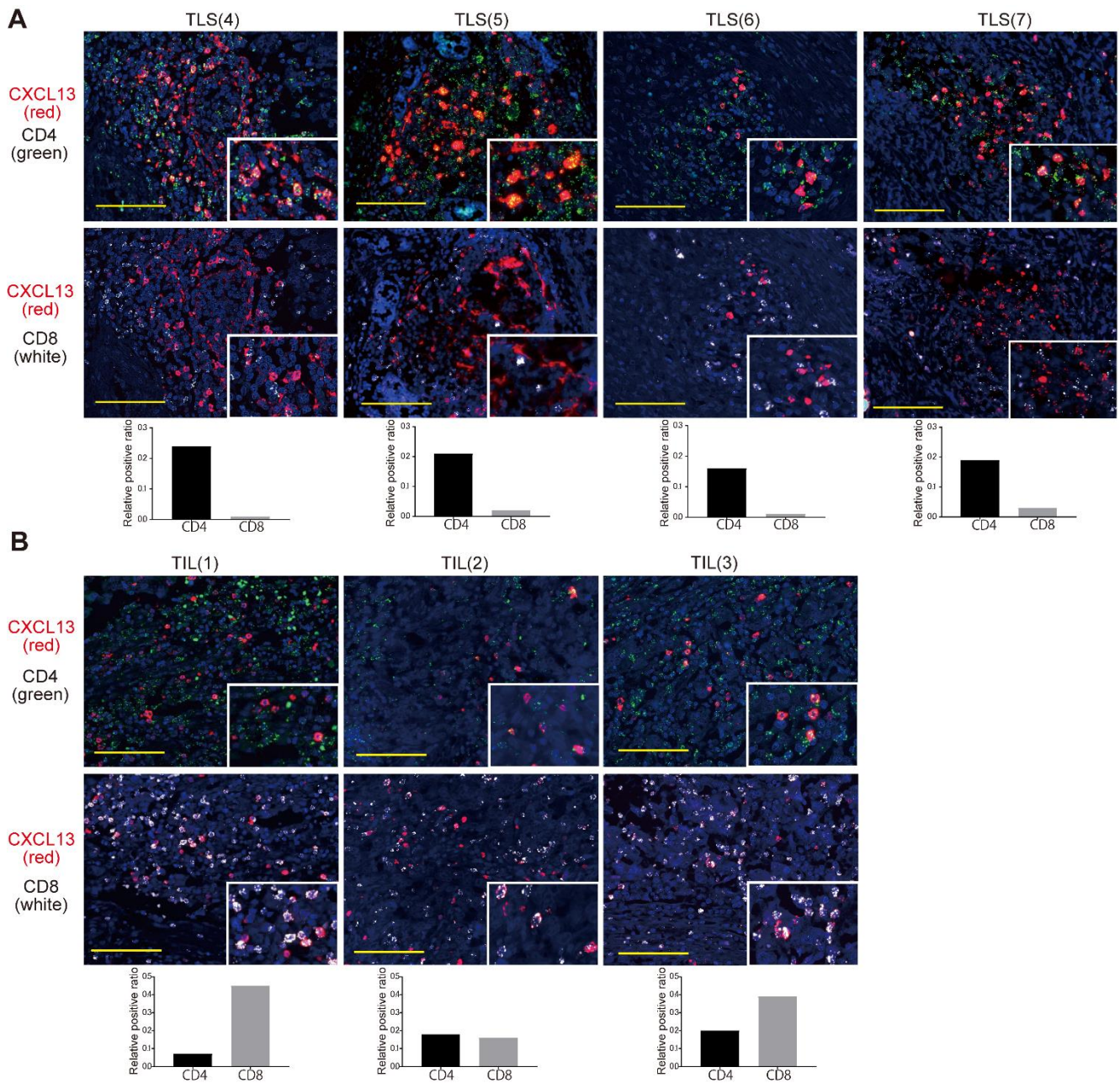


629

630 **Figure 2. CXCL13 gene expression in tumors correlates with TLS formation, lymphocyte infiltration, and a**  
 631 **favorable prognosis for ovarian cancer. (A)** Representative TLS in tissues stained by H&E and CXCL13 (Fast  
 632 RED) by RNA ISH. Scale bars indicate 100  $\mu$ m. **(B)** TLS presence ratio based on CXCL13 gene expression. Analysis  
 633 by Fisher's exact test in 28 cases with microarray data. **(C)** Characterization of the immune infiltrate in tumors  
 634 according to CXCL13 gene expression (n=28). Correlation was determined by Spearman's correlation test. **(D)** **(E)**  
 635 The distribution of infiltrating immune cells into the tumor site and CXCL13 gene expression using CIBERSORT  
 636 (n=522). Correlation was determined by Spearman's correlation test. **(F)** Overall survival of patients with HGSC by

637 CXCL13 gene expression (TCGA n=217, KOV n=28). Patients with CXCL13 high defined if CXCL13 gene  
638 expression was above the median. Analyses were performed with Kaplan-Meier estimates, log-rank tests and  
639 Wilcoxon tests. The level of significance was set as  $*P<0.05$ ,  $**P<0.01$ , and  $****P<0.0001$ .  
640

641



642

643 **Figure 3. CXCL13 is mainly produced by CD4<sup>+</sup> T cells in TLS.** (A) Fluorescent double staining of CXCL13 (red)

644 and CD4 (green), and CXCL13 (red) and CD8 (white) by RNA ISH in TLS. Images of four representative TLS are

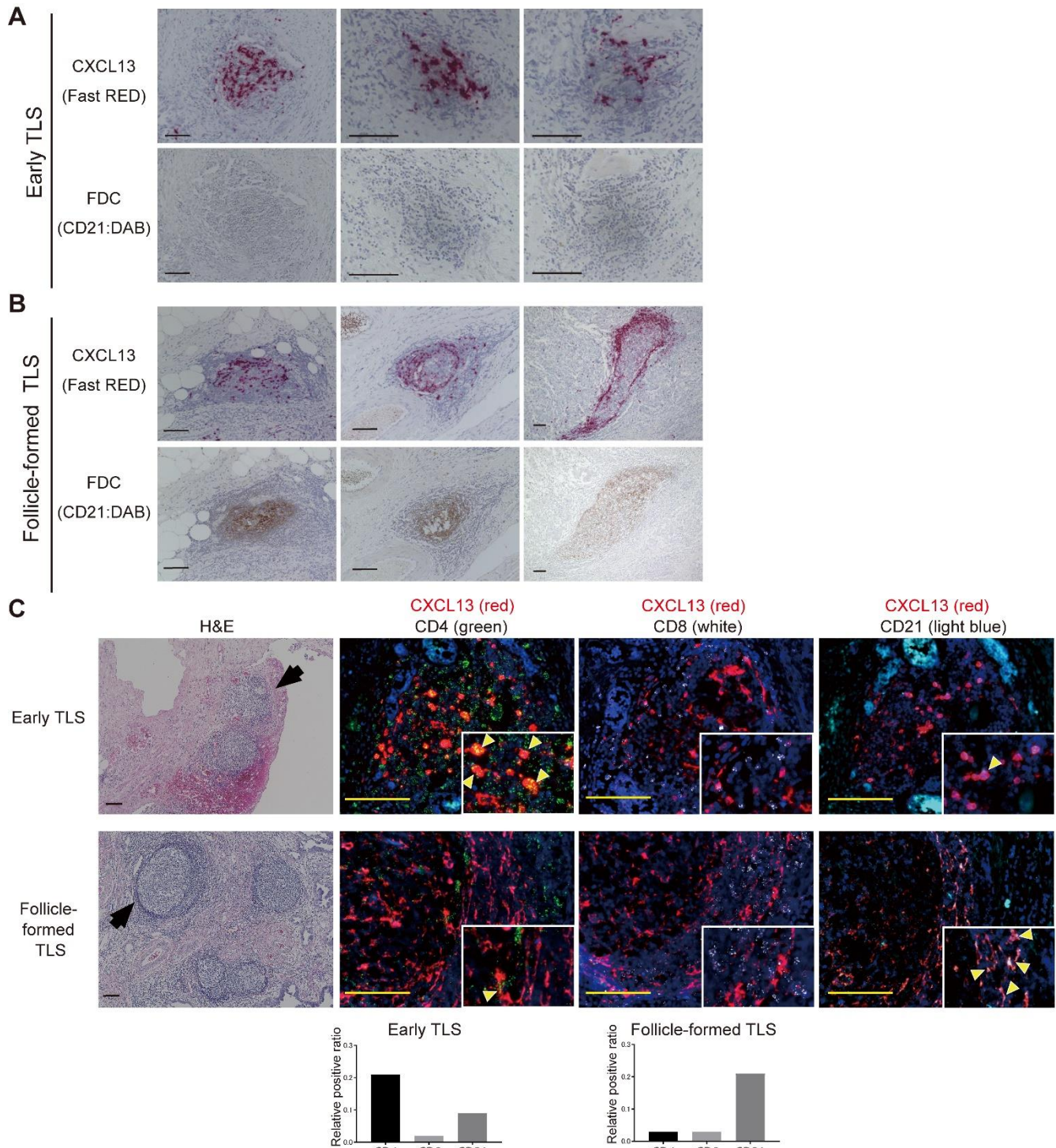
645 shown. (B) Fluorescent double staining of CXCL13 (red) and CD4 (green), and CXCL13 (red) and CD8 (white) by

646 RNA ISH in TIL. The upper and lower pictures are representative TIL images from the same patient. Nuclei are

647 stained with DAPI (blue). Scale bars indicate 100  $\mu$ m. Co-localization of CXCL13 with CD4 or CD8 is shown in the

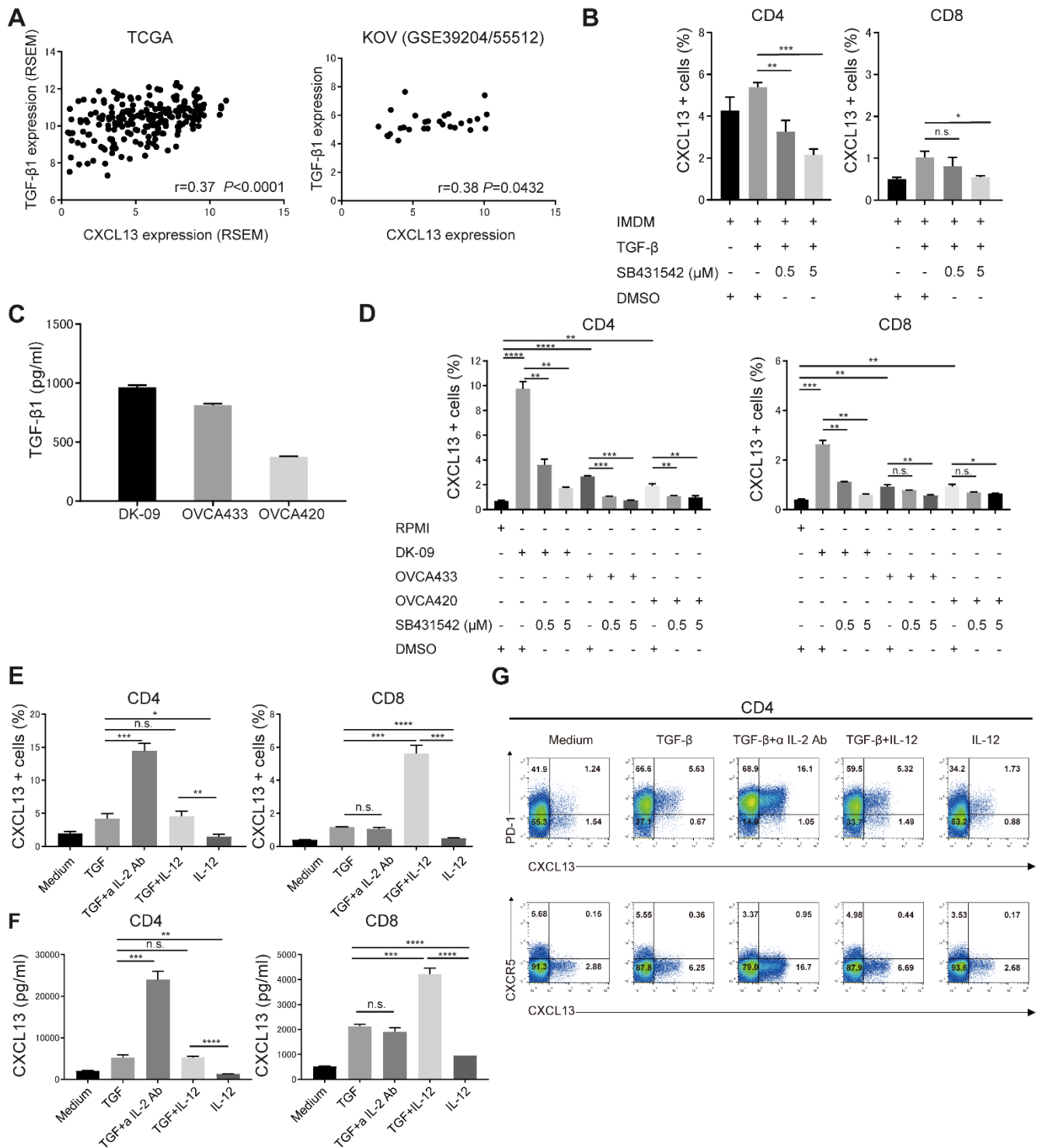
648 bar graph as the relative positive ratio quantified using BZ-H4C/hybrid cell count software.

649



650

651 **Figure 4. The source of CXCL13 production in TLS shifts to CD21<sup>+</sup> FDC with the maturation of TLS. (A)**  
 652 **Representative images of early TLS. (B) Representative images of follicle-formed TLS. Upper panels show CXCL13**  
 653 **(RNA ISH, Fast RED) and lower panels show FDC (CD21 IHC, DAB). (C) Fluorescence double staining of CXCL13**  
 654 **(red) and CD4 (green), CXCL13 (red) and CD8 (white), and CXCL13 (red) and CD21 (light blue) in representative**  
 655 **early TLS and follicle-formed TLS. Nuclei are stained with DAPI (blue). Scale bar indicates 100 μm. Co-localization**  
 656 **of CXCL13 with CD4, CD8, or CD21 is shown in the bar graph as the relative positive ratio quantified using BZ-**  
 657 **H4C/hybrid cell count software.**



658

659

660

661

662

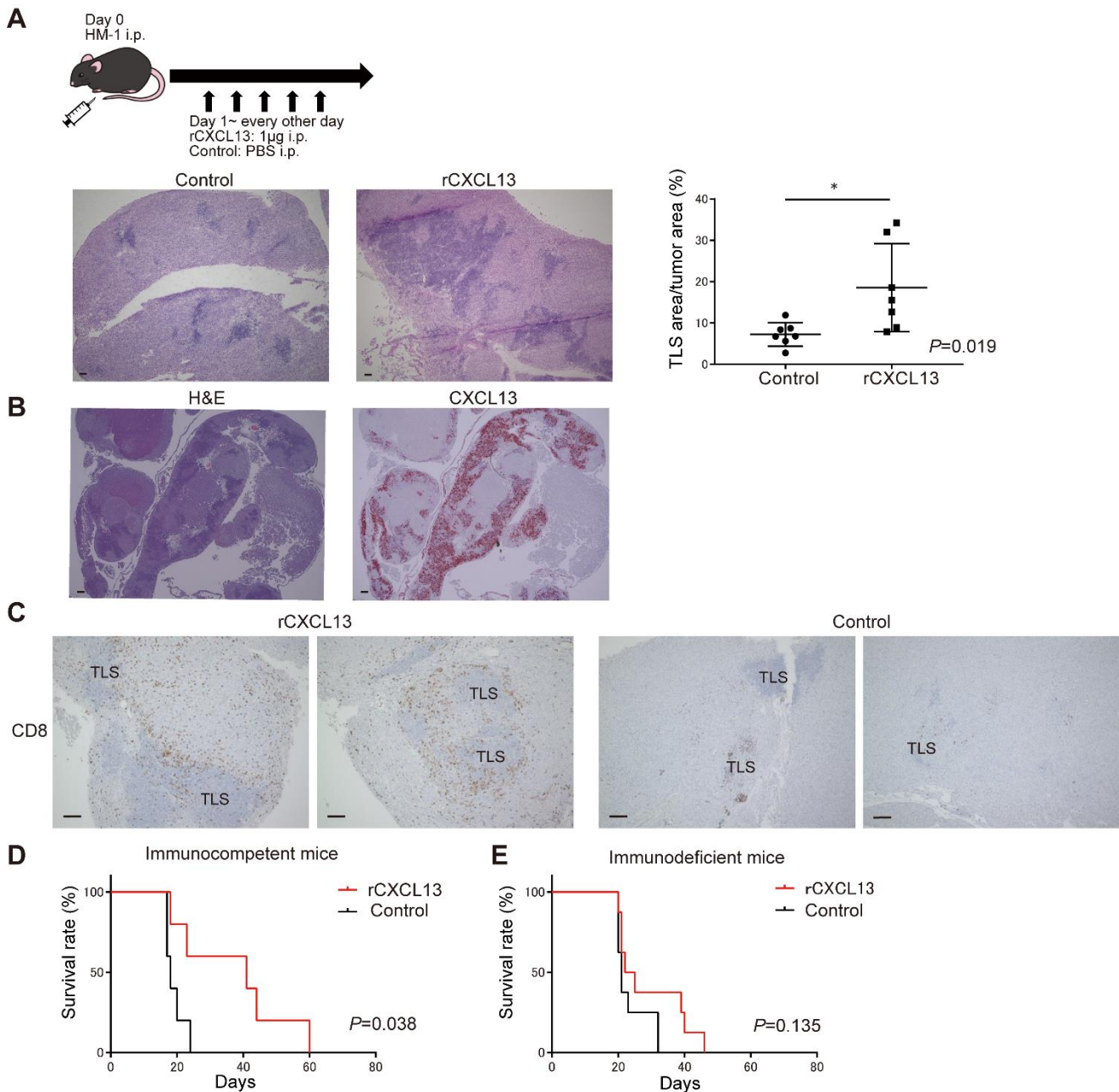
663

664

665

**Figure 5. TGF- $\beta$  promotes the production of CXCL13.** (A) Correlation between CXCL13 and TGF- $\beta$ 1 expression in TCGA (n=217) and KOV (n=28). Correlation was determined by Spearman's correlation test. (B) Human naive CD4<sup>+</sup> and CD8<sup>+</sup> T cells from a healthy donor were differentiated by TCR stimulation and TGF- $\beta$ 1 in the presence or absence of a TGF signal inhibitor, SB431542. The proportion of CXCL13<sup>+</sup> cells was determined by flow cytometry. Data are shown as the mean  $\pm$  SEM of four samples. Statistical significance was determined by two-tailed Student's *t*-test, \**P*<0.05, \*\**P*<0.01, \*\*\**P*<0.001, n.s.: not significant. (C) The concentration of TGF- $\beta$ 1 in conditioned medium obtained from three human ovarian cancer cell lines was measured by ELISA. Data are shown as the mean

666 ± SEM of three samples. **(D)** Human naïve CD4<sup>+</sup> and CD8<sup>+</sup> T cells from a healthy donor were differentiated with  
667 TCR stimulation and conditioned medium obtained from three human ovarian cancer cell lines in the presence or  
668 absence of a TGF signal inhibitor, SB431542. The proportion of CXCL13<sup>+</sup> cells was determined by flow cytometry.  
669 Data are shown as the mean ± SEM of triplicates. **(E) (F) (G)** Human naïve CD4<sup>+</sup> and CD8<sup>+</sup> T cells from a healthy  
670 donor were differentiated with TCR stimulation and the indicated cytokines. The proportion of CXCL13<sup>+</sup> cells was  
671 determined by flow cytometry **(E)**. The concentration of CXCL13 in the culture supernatant was measured by ELISA  
672 **(F)**. Data are shown as the mean ± SEM of four samples in CD4 and three samples in CD8. Statistical significance  
673 was determined by two-tailed Student's *t*-test, \**P*<0.05, \*\**P*< 0.01, \*\*\**P*< 0.001, \*\*\*\**P*<0.0001, n.s.: not significant.  
674 Representative dot plots of PD-1 (upper row), CXCR5 (lower row), and intracellular CXCL13 in healthy human  
675 naïve CD4<sup>+</sup> T cells are shown **(G)**. a IL-2 Ab indicates anti IL-2 antibody.  
676



677

678 **Figure 6. Mouse recombinant CXCL13 induces TLS in tumors and prolongs survival.** (A) Mouse rCXCL13 was  
 679 administered intraperitoneally to induce TLS in a mouse ovarian cancer model. Representative H&E images of TLS  
 680 formed in an omental tumor. The area of TLS per tumor area was compared between the control group and the  
 681 rCXCL13 treated group (n=7, each). Statistical significance was determined by two-tailed Student's *t*-test, \* $P<0.05$ .  
 682 (B) TLS induced by mouse rCXCL13 (H&E) and expression of mouse CXCL13 corresponding to TLS (RNA ISH,  
 683 Fast RED). (C) CD8<sup>+</sup> T cell IHC images (DAB) in the rCXCL13 treated group and control group. Scale bars indicate  
 684 100 µm. (D) (E) The effect of rCXCL13 administration on the survival of tumor-bearing mice was compared between  
 685 immunocompetent mice (D) and immunodeficient mice (E). Analyses were performed using Kaplan-Meier estimates  
 686 and log-rank tests.